Aerodynamic Characteristics and Development of the Aerodynamic Database of the X-34 Reusable Launch Vehicle

Bandu N. Pamadi and Gregory J. Brauckmann
NASA Langley Research Center
Hampton, VA 23681

International Symposium on
Atmospheric Reentry Vehicles and Systems
March 16-18, 1999
Arcachon, France

Aerodynamic Characteristics and Development of the Aerodynamic Database of the X-34 Reusable Launch Vehicle

By

Bandu N.Pamadi[1] and Gregory J. Brauckmann[2]
NASA Langley Research Center, Hampton, VA 23681

Abstract

An overview of the aerodynamic characteristics and the process of developing the preflight aerodynamic database of the NASA/ Orbital X-34 reusable launch vehicle is presented in this paper. Wind tunnel tests from subsonic to hypersonic Mach numbers including ground effect tests at low subsonic speeds were conducted in various facilities at the NASA Langley Research Center. The APAS (Aerodynamic Preliminary Analysis System) code was used for engineering level analysis and to fill the gaps in the wind tunnel test data. This aerodynamic database covers the range of Mach numbers, angles of attack, sideslip and control surface deflections anticipated in the complete flight envelope.

Nomenclature

b	Wing span
C_D	Drag coefficient
C_L	Lift coefficient
C_l	Rolling-moment coefficient
C_m	Pitching-moment coefficient
C_n	Yawing-moment coefficient
C_Y	Side-force coefficient
h	Height of the moment reference point above the ground plane, ft
M	Mach number
α	Angle of attack, deg
β	Angle of sideslip, deg
δ_a	Aileron deflection angle, deg
δ_e	Elevon deflection angle, deg
δ_{bf}	Bodyflap deflection angle, deg
δ_r	Rudder deflection angle, deg
δ_{sb}	Speedbrake deflection angle, deg

[1] Aerospace Engineer, Vehicle Analysis Branch
[2] Aerospace Engineer, Aerothermodynamics Branch

Introduction

The X-34 vehicle being developed by the Orbital Sciences Corporation (OSC) for National Aeronautics and Space Administration (NASA) is an integral part of the reusable launch vehicle (RLV) technology program currently being pursued by NASA with industry partnership. A schematic representation of the RLV technology demonstration path is shown in Figure 1. The primary goal of the RLV program [1] is to develop key technologies needed to successfully build and operate reusable space transportation systems that will significantly lower the cost of access to space. The X-34 program originally started in Spring of 1995 when the team of OSC and Rockwell International was awarded a NASA contract to build an unmanned, fully reusable, two-stage, orbital vehicle capable of delivering about 1500 lb to low earth orbit. However, this program was cancelled in late 1995 when OSC and Rockwell determined that the program was not economically feasible. This program was resurrected in

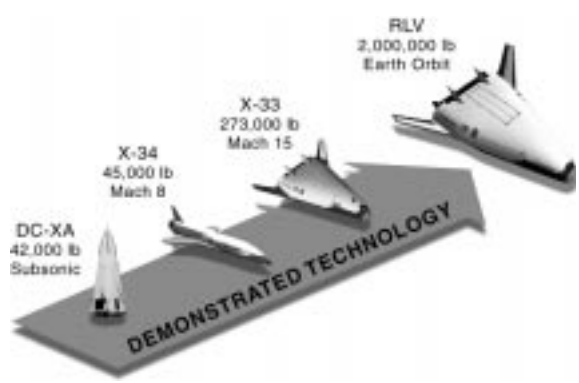

Figure 1. RLV technology demonstration path.

Spring of 1995 when NASA solicited proposals on a different vehicle, also designated X-34 [2]. OSC (now Orbital) was awarded this contract in June 1996.

The current X-34 vehicle is an unmanned sub-orbital, technology demonstrator vehicle capable of reaching an altitude of 250,000 ft and a speed of Mach 8. Some of the key technologies related to RLV that will be demonstrated by the X-34 vehicle include primary and secondary composite structures, advanced thermal protection systems (TPS), low cost avionics, rapid turn around times, autonomous flight including landing and all weather airplane-like operations.

The NASA Langley Research Center is involved in the development of the preflight aerodynamic database of the X-34 vehicle. Towards this objective, Langley has conducted wind tunnel tests from subsonic to hypersonic speeds including ground effect tests at low subsonic speeds and performed extensive analysis using an engineering level code called APAS (Aerodynamic Preliminary Analysis System). Also, some limited CFD efforts have addressed the issue of the variation of aerodynamic coefficients from wind tunnel to full scale flight Reynolds numbers. The objective of this paper is to present an overview of this activity, and discuss some of the salient aerodynamic characteristics of the X-34 vehicle. However, this discussion is limited to static aerodynamic forces and moments in free flight and in ground effect, and does not include aerodynamic uncertainties, control surface hinge moments, dynamic stability parameters, aeroelastic effects and the reaction control systems that may be used on the X-34 flight vehicle.

Vehicle/Mission Description

The X-34 vehicle has a close similarity with the Space Shuttle Orbiter but is relatively smaller in size. It has an overall length of about 58 ft, wing span of 28 ft and a height of about 12 ft. The approximate gross weight of the vehicle is 45000 lb. The main wing has a leading edge sweepback of 45°, a dihedral of 6°, and 80° leading edge strake. It has full span split elevons. However, the elevons on the same side are always deflected together. Deflected symmetrically, elevons provide pitch control and asymmetric deflections provide roll control. It also features a centerline, all movable vertical tail for directional stability/control. The vertical tail has a split speedbrake for energy management during descent. The vehicle has a bodyflap located at the trailing edge of the fuselage. The bodyflap helps to shield the engine nozzle from aerodynamic heating at hypersonic speeds and also augments pitch control. The TPS system on X-34 consists of a mix of ceramic tiles and blankets [3]. Ceramic tiles are used in the stagnation regions of the nose and wing leading edges where the aerodynamic heating is quite severe. Three types of blankets are employed for the rest of the acreage of the vehicle. The so called HT-FRSI (High Temperature Flexible Reusable Surface Insulation) blankets are used where the surface temperatures may reach as high as 2000°F. The second type of blanket called AFRSI (Advanced FRSI) is used where the surface temperatures are not expected to exceed 1500°F and the third type of blanket called FRSI is used where the surface temperatures are expected to be lower than 700°F.

The X-34 will be powered by the "Fastrac" rocket engine which is currently under development at the NASA Marshall Space Flight Center, Huntsville, Alabama. The bi-propellent (liquid oxygen (LOX)/kerosene) Fastrac engine is designed for a nominal thrust of 60,000 lb and is expected to have a thrust vectoring capability of ±15°.

A typical X-34 mission profile is depicted in Figure 2. The X-34 vehicle will be "captive" carried under the belly of the L-1011 aircraft up to an altitude of about 38,000 ft and a Mach number of 0.7 at which point it will be released. The vehicle will be unpowered and all its control surfaces will be locked for the first 5 or 6 seconds following the drop. Once

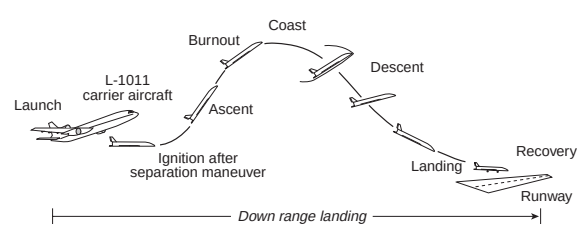

Figure 2. Typical X-34 flight profile.

the vehicle makes a safe separation from the L-1011 aircraft, the Fastrac engine will ignite and accelerate the vehicle towards its target altitude of 250,000 ft and target speed of Mach 8. After engine burnout, the vehicle will coast and glide back to earth and execute an autonomous, airplane-type landing on a conventional runway.

At drop, the vehicle center of gravity is located approximately 421 in from the fuselage nose. During ascent as the propellants are consumed, the center of gravity initially moves aft to 432 in and then moves forward to 414 in at the end of the ascent phase and then remains at that location for the rest of the flight which consists of a glide back to earth. This pattern of center of gravity movement is due to the manner in which the LOX is consumed. The vehicle has two LOX tanks, one located forward and the other aft. The LOX is consumed first from the forward tank causing the center of gravity to move aft and then from the aft tank causing the center of gravity to move forward.

Typical variations of the altitude, angle of attack and Mach number along a nominal trajectory called "DRM2 (X1005026)" are shown in Figure 3. During the initial phase of the ascent, the angle of attack reaches a value of about 13° so that the vehicle climbs rapidly out of the lower layers of the earth's atmosphere in order to keep the aerodynamic loads on the vehicle as low as possible. Subsequently, the angle attack decreases and remains in the range of 5° to 10° for the remaining part of the

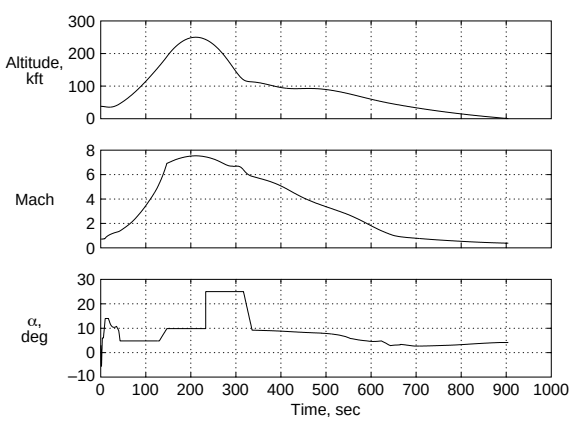

Figure 3. Nominal flight trajectory of the X-34 vehicle.

ascent. On return, the vehicle maintains an angle of attack of about 25° for the hypersonic part of the descent during which it is subjected to severe aerodynamic heating. The angle of attack decreases steadily as the vehicle decelerates to low subsonic speeds. Finally, the vehicle will land on a runway with an approximate speed of Mach 0.3.

The flight testing of the X-34 vehicle is expected to commence in March 1999 starting with L-1011 captive carry tests. These will be followed by unpowered drop tests in the fall of 1999. Powered flight tests are expected to commence in the spring of the year 2000.

Wind Tunnel Test Facilities

A brief description of the various wind tunnel facilities used in generating the test data on the X-34 configuration from subsonic to hypersonic speeds is presented in the following paragraphs. Additional information on these test facilities may be found in [4,5,6,7].

LaRC 14- by 22-Foot Subsonic Tunnel

The Langley 14- by 22-Foot Subsonic Tunnel is a closed circuit, single return, atmospheric tunnel with a maximum speed of 338 ft/sec. The test section measures 14.5- by 21.8 ft and has a length of about 50 ft. The maximum unit Reynolds number is 2.1×10^6 per ft. This tunnel can be operated in a variety of modes such as a closed tunnel or with slotted walls or as one or more open configurations by removing side walls and the ceiling. The tunnel is equipped with boundary layer suction on the floor at the entrance to the test section and a moving ground-belt ground board for ground effect tests. It features a large model preparation area, adjacent to the wind tunnel for model assembly and disassembly.

LaRC 16-Foot Transonic Tunnel

The Langley 16-Foot Transonic Tunnel is a closed circuit, single return, continuous flow atmospheric tunnel. The test medium is air. This tunnel has a slotted wall, octagonal test section which measures 15.5 ft across the flats. The normal test Mach number ranges from 0.3 to 1.3. The angle of

attack can be varied up to 25°. The unit Reynolds number varies from 2.0 to 4 x 10^6 per ft. The usable length of the test section varies with test Mach number. It is about 22 ft for Mach numbers up to 1.1 but reduces to 8 ft for Mach numbers above 1.1.

LaRC Unitary Plan Wind Tunnel

The LaRC Unitary Plan Wind Tunnel (UPWT) is a continuous flow, variable pressure, closed circuit pressure tunnel having two separate test sections, called low Mach number test section and high Mach number test section. Each test section measures 4- by 7-ft. The tunnel is capable of operating from near vacuum conditions to a pressure of 10 atmospheres. The low Mach number test section covers the Mach number range from 1.46 to 2.86 and the high Mach number test section from 2.3 to 4.6. The angle of attack capability is from –12° to 22° with possibility for testing at higher values using dogleg strings. The sideslip range is from –4° to +4°.

LaRC 20-Inch Mach 6 Wind Tunnel

The LaRC 20-Inch Mach 6 Tunnel is a blow down test facility that uses heated, dried and filtered air as test medium. The test section measures 20.5- by 20-inches. Typical operating stagnation pressures range from 30 to 500 psi and the stagnation temperature from 750° to 1000° R. The unit test Reynolds number are in the range of 0.5 to 8 x 10^6 per ft. This tunnel has a capability to run continuously up to 15 minutes. The tunnel is equipped with a model injection system on the bottom of the test section that can insert a sheltered model into the air stream in less than 0.5 seconds.

Models, Instrumentation and Test Procedure

The test model for the 14-ft by 22-ft low subsonic, freestream and ground effect tests was a 0.1-scale model of the X-34 OML (Outer Mold Line, inclusive of TPS) geometry.

In the 14-ft by 22-ft wind tunnel, both freestream and ground effect tests were conducted. The freestream tests were done for clean configuration (landing gear fully retracted and doors closed) as well as configuration with landing gear extended. The ground effect tests were conducted with and without landing gear extended. The boundary layer suction was used but the moving-belt ground board was not used in the X-34 ground effect tests. The X–34 vehicle has two main gear doors per gear and a single nose gear door. Thus, when the nose gear is down and its door is open, the configuration becomes aerodynamically asymmetric. Tests were conducted for various combinations of main gear, nose gear extended/retracted and their doors open/closed to cover various gear deployment sequences during approach and landing. The ground effect test data was obtained for various separation heights (measured from moment reference point to the ground plane) ranging from 0.3 to 2.5 times wing span. A photograph of the X-34 model in 14-by 22-Ft Subsonic Tunnel is shown in Figure 4.

Figure 4. Photographs of 0.1 scale model of the X-34 vehicle in 14- by 22-Foot Subsonic Tunnel.

The model for the 16-Foot Transonic tunnel and the Unitary Plan Wind Tunnel was a 0.033-scale model of the X-34 OML geometry. The model for the 20-Inch Mach 6 test was a 0.0183-scale model of the X-34 OML geometry.

The aerodynamic forces and moments were measured with a six component strain gage balance. Three different balances were used to manage the load ranges encountered in the different test facilities. Further, the balance used in the 20-Inch Mach 6 tests was water cooled to minimize the balance tem-

perature variations due to aerodynamic heating. Due to various limitations imposed by the fast pace of this program, it was not possible to perform any pressure measurements or flow visualization on any of the models in any of the test facilities.

The force and moment data was acquired in a pitch and pause manner. The base and cavity pressures were measured on all the models. The 0.033-scale model had pressure taps in the base and the 0.0183-scale model for Mach 6 test had external pressure tubes that ran along side the sting. Using these pressure measurements, the correction to the measured axial force was determined. For the test models in the 16-Foot transonic tunnel and the UPWT low Mach number tests, the boundary layer transition trips were applied to the nose, wing and vertical tail leading edges to promote turbulent flow over the test models. The test models in 20-Inch Mach 6 tunnel and in UPWT high Mach number tests were not tripped.

In general, the tests in all the above facilities covered elevon deflections (symmetric) from –30° to +20°, aileron deflections of –30° to 20° (left elevon deflected, right held at zero), bodyflap deflections of –15° to +20°, rudder deflection of 5° to 30° and nominal speedbrake deflections of 30° to 90°. For subsonic and low supersonic tests (up to Mach 2.5), the angle of attack varied from –4° to 20°. For higher Mach numbers, the angle of attack reached up to 36°. In general, the sideslip for all the tests was in the range of –6° to 6°. The moment reference point was located 420 in from the nose. All the aerodynamic data presented in this paper is with respect to this moment reference point.

The uncertainties in the balance measurement were estimated as follows: for Mach number ranging from 0.3 to 6.0, normal force from 0.001 to 0.0216, axial force from 0.0008 to 0.0054, pitching moment coefficient from 0.004 to 0.009, side force coefficient from 0.0028 to 0.0179, rolling moment coefficient from 0.0005 to 0.0011 and the yawing moment coefficient from 0.0008 to 0.004. These are the wind tunnel measurement uncertainties and not the aerodynamic uncertainties for the data in the aerodynamic database. Additional information on the measurement uncertainties can be found in [8].

Analysis Method

The aerodynamic analysis of the X-34 vehicle was performed using APAS (Aerodynamic Preliminary Analysis System) which is an interactive computer code developed jointly by NASA Langley and Rockwell (now part of Boeing) in the early 80's [9,10]. As the name implies, this code is a preliminary analysis tool capable of providing quick estimates of complete aerodynamic characteristics of aerospace configurations from subsonic to hypersonic speeds including control surface deflections. Computationally, APAS run times are of the order of minutes so that the aerodynamic characteristics of a given aerospace configuration can be generated in matters of hours as opposed to several days or weeks required by higher fidelity CFD methods. On account of this unique capability, APAS still remains an useful aerodynamic tool for conceptual level analysis and preliminary design studies.

In subsonic and low supersonic regimes, APAS utilizes a combination of slender- body theory, source and vortex panel distributions, and empirical viscous and wave drag estimating methods. The fuselage type components are analyzed by the slender-body theory. The lifting surfaces such as wings and tails are analyzed by a panel method that uses distributions of linear sources and vortices. The mutual interference between the fuselage and lifting surfaces is accounted for through a cylindrical interference shell enveloping the fuselage. The subsonic/low supersonic analysis in APAS is performed by the UDP (Unified Distributed Panel) code.

For high supersonic/hypersonic speeds, APAS utilizes the Mark III HABP (Hypersonic Arbitrary Body Program). The HABP code uses the same geometry model as that used for subsonic/low supersonic analysis. The HABP module has various analysis options like tangent cone, tangent wedge, Newtonian impact methods etc.

Generally, APAS gives good results for longitudinal aerodynamic coefficients at subsonic, supersonic and hypersonic speeds. The APAS predictions are particularly good at hypersonic speeds. The pitching moment coefficient may some times differ from high fidelity wind tunnel tests or CFD methods

especially for configurations with long fuselages and with aft center of gravity locations. For such configurations, empirical adjustments to APAS usually result in satisfactory predictions of the pitching moment coefficient. At transonic speeds, the APAS predictions are known to differ from wind tunnel test data. The APAS predictions of lateral/directional aerodynamic coefficients are generally of the first order accuracy. The side force and rolling moment coefficient predictions are satisfactory for wing-body type configurations. However, the yawing moment coefficient can be considerably in error especially for body dominated configurations. Examples of APAS application to aerospace configurations can be found in [11,12,13].

An APAS geometry model of the X-34 vehicle is shown in Figure 5.

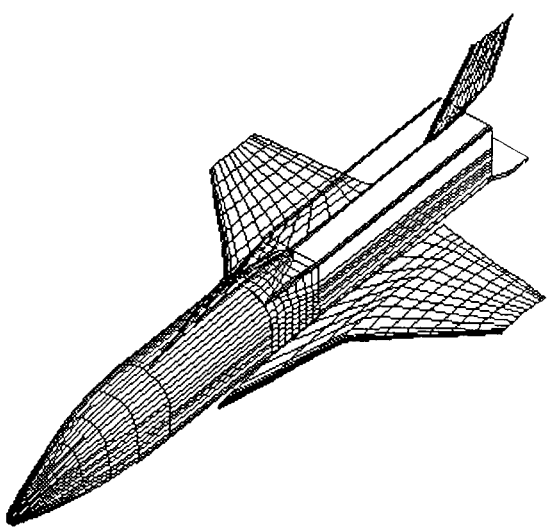

Figure 5. APAS geometry model of the X-34 vehicle.

Formulation of Aerodynamic Database

An important aspect of developing an aerodynamic database is the formulation of an aerodynamic model. The accuracy of the database depends on the degree to which the aerodynamic model represents the physics of the problem. Therefore, it is important that all the aerodynamic and control variables that may have an influence on the given aerodynamic coefficient must be included in the aerodynamic model. This could be an iterative process because the wind tunnel test data may display some variations that were not initially included in the aerodynamic model. In the following, we discuss the development of an aerodynamic model for the X-34 vehicle for the evaluation of the static aerodynamic forces and moments in free flight and for flight in ground effect.

Aerodynamic Coefficients in Free Flight

By free flight, we mean that the vehicle is not influenced by the ground. This assumption generally holds when the vehicle is at a height exceeding 2.5 wing spans. To begin with, assume that the lift coefficient is given by

$$\begin{aligned} C_{L,total} = {} & C_{L,b}(\alpha, M) + \Delta C_{L,\delta_e} + \Delta C_{L,\delta_a} + \Delta C_{L,\delta_{bf}} \\ & + \Delta C_{L,\delta_r} + \Delta C_{L,\delta_{sb}} + \Delta C_{L,LG} + \Delta C_{L,b,\beta} \\ & + \Delta C_{L,\delta_r,\beta} + \Delta C_{L,\delta_{sb},\beta} + \Delta C_{L,LG,\beta} \end{aligned} \tag{1}$$

This formulation is similar to that used in the Space Shuttle data book [14]. Here, $C_{L,total}$ is the total coefficient of the vehicle for a given flight condition as expressed by the flight Mach number M, angle of attack α, sideslip β, elevon deflection δ_e (symmetric), ailerons deflections δ_a (asymmetric), bodyflap deflection δ_{bf}, rudder deflection δ_r, and speedbrake opening δ_{sb}. In this formulation, the mutual aerodynamic interference between various control surfaces is ignored. The parameter $C_{L,b}(\alpha,M)$ is baseline lift coefficient in zero sideslip and zero control surface deflections. The parameter $\Delta C_{L,\delta_e}$ represents incremental lift coefficient due to symmetric elevon deflections above the baseline and is given by

$$\Delta C_{L,\delta_e} = C_L(\alpha, M, \delta_e) - C_{L,b}(\alpha, M) \tag{2}$$

The parameter $\Delta C_{L,\delta_a}$ represents the incremental lift coefficient due to aileron (asymmetric elevons) deflections above the baseline and can be evaluated using the data on symmetric elevons as follows:

$$\begin{aligned} \Delta C_{L,\delta_a} = {} & 0.5(\Delta C_{L,\delta_e=\delta_{e,L}} + \Delta C_{L,\delta_e=\delta_{e,R}}) \\ & - \Delta C_{L,\delta_e} \end{aligned} \tag{3}$$

Here, we use the elevon data twice, once assuming $\delta_e = \delta_{e,L}$, obtain $\Delta C_{L,\delta_e=\delta_{e,L}}$ and then assuming $\delta_e = \delta_{e,R}$, determine $\Delta C_{L,\delta_e=\delta_{e,R}}$. This approach is similar to that done in the shuttle data book [14]. As

a check, when aileron deflection is zero, i.e., $\delta_{e,L} = \delta_{e,R}$, the value of $\Delta C_{L,\delta_a}$ given by equation (3) vanishes as expected.

The incremental lift coefficients $\Delta C_{L,\delta_{bf}}$, $\Delta C_{L,\delta_r}$, $\Delta C_{L,\delta_{sb}}$ due to bodyflap, rudder and speedbrake are defined as follows:

$$\Delta C_{L,\delta_{bf}} = C_L(\alpha, M, \delta_{bf}) - C_{L,b}(\alpha, M) \tag{4}$$

$$\Delta C_{L,\delta_r} = C_L(\alpha, M, \delta_r) - C_{L,b}(\alpha, M) \tag{5}$$

$$\Delta C_{L,\delta_{sb}} = C_L(\alpha, M, \delta_{sb}) - C_{L,b}(\alpha, M) \tag{6}$$

$$\Delta C_{L,LG} = C_L(\alpha, M, LG) - C_{L,b}(\alpha, M) \tag{7}$$

The incremental lift coefficients due to baseline, rudder, speedbrake and landing gear (LG) in sideslip are given by

$$\Delta C_{L,b,\beta} = C_L(\alpha, M, \beta) - C_L(\alpha, M) \tag{8}$$

$$\begin{aligned}\Delta C_{L,\delta_r,\beta} &= [C_L(\alpha, M, \beta, \delta_r) - C_L(\alpha, M, \beta)] \\ &\quad - \Delta C_{L,\delta_r}\end{aligned} \tag{9}$$

$$\begin{aligned}\Delta C_{L,\delta_{sb},\beta} &= [C_L(\alpha, M, \beta, \delta_{sb}) - C_L(\alpha, M, \beta)] \\ &\quad - \Delta C_{L,\delta_{sb}}\end{aligned} \tag{10}$$

$$\begin{aligned}\Delta C_{L,LG,\beta} &= [C_L(\alpha, M, \beta, LG) - C_L(\alpha, M, \beta)] \\ &\quad - \Delta C_{L,LG}\end{aligned} \tag{11}$$

Observe that the first term in square brackets on the right hand side of equation (9) gives the combined incremental coefficient due to rudder at an angle of attack and sideslip over the baseline at the same values of angle of attack and sideslip. To get the incremental coefficient due only to sideslip β, we have to subtract the incremental due to angle of attack as shown by the second term on the right hand side of equation (9). A similar explanation applies to equations (10) and (11).

The above incremental lift coefficients for baseline, rudder, speedbrake and landing gear in sideslip represent aerodynamic cross coupling effects. These terms are included in the X-34 aerodynamic model because they were found to assume significance, especially at higher values of angles of attack.

In a similar fashion, we assume that the drag and pitching moment coefficients are given by,

$$\begin{aligned}C_{D,total} &= C_{D,b}(\alpha, M) + \Delta C_{D,\delta_e} + \Delta C_{D,\delta_a} + \Delta C_{D,\delta_{bf}} \\ &\quad + \Delta C_{D,\delta_r} + \Delta C_{D,\delta_{sb}} + \Delta C_{D,LG} + \Delta C_{D,b,\beta} \\ &\quad + \Delta C_{D,\delta_r,\beta} + \Delta C_{D,\delta_{sb},\beta} + \Delta C_{D,LG,\beta}\end{aligned} \tag{12}$$

$$\begin{aligned}C_{m,total} &= C_{m,b}(\alpha, M) + \Delta C_{m,\delta_e} + \Delta C_{m,\delta_a} + \Delta C_{m,\delta_{bf}} \\ &\quad + \Delta C_{m,\delta_r} + \Delta C_{m,\delta_{sb}} + \Delta C_{m,LG} + \Delta C_{m,b,\beta} \\ &\quad + \Delta C_{m,\delta_r,\beta} + \Delta C_{m,\delta_{sb},\beta} + \Delta C_{m,LG,\beta}\end{aligned} \tag{13}$$

The side force coefficient is assumed to be given by

$$\begin{aligned}C_{Y,total} &= C_{Y,b}(\alpha, M) + \Delta C_{Y,b,\beta} + \Delta C_{Y,\delta_a} \\ &\quad + \Delta C_{Y,\delta_r} + \Delta C_{Y,LG} + \Delta C_{Y,\delta_r,\beta} \\ &\quad + \Delta C_{Y,\delta_{sb},\beta} + \Delta C_{Y,LG,\beta}\end{aligned} \tag{14}$$

Note that $C_{Y,b}(\alpha,M) = 0$ due to symmetry. Further,

$$\begin{aligned}\Delta C_{Y,b,\beta} &= C_{Y,b}(\alpha, \beta, M) - C_{Y,b}(\alpha, M) \\ &= C_{Y,b}(\alpha, \beta, M)\end{aligned} \tag{15}$$

Similarly,

$$\Delta C_{Y,\delta_a} = C_Y(\alpha, M, \delta_a) \tag{16}$$

$$\Delta C_{Y,\delta_r} = C_Y(\alpha, M, \delta_r) \tag{17}$$

$$\Delta C_{Y,\delta_{sb}} = C_Y(\alpha, M, \delta_{sb}) \tag{18}$$

$$\Delta C_{Y,LG} = C_Y(\alpha, M, LG) \tag{19}$$

Then,

$$\begin{aligned}C_{Y,total} &= C_{Y,b}(\alpha, \beta, M) + C_Y(\alpha, M, \delta_a) \\ &\quad + C_Y(\alpha, M, \delta_r) + C_Y(\alpha, M, \delta_{sb}) \\ &\quad + C_Y(\alpha, M, LG) + \Delta C_{Y,\delta_r,\beta} \\ &\quad + \Delta C_{Y,\delta_{sb},\beta} + \Delta C_{Y,LG,\beta}\end{aligned} \tag{20}$$

The incremental side force coefficients due to rudder, speedbrake and landing gear deployment in sideslip are defined as

$$\Delta C_{Y,\delta_r,\beta} = [C_Y(\alpha,\beta,M,\delta_r) - C_{Y,b}(\alpha,\beta,M)] - \Delta C_{Y,\delta_r} \tag{21}$$

$$\Delta C_{Y,\delta_{sb},\beta} = [C_Y(\alpha,\beta,M,\delta_{sb}) - C_{Y,b}(\alpha,\beta,M)] - \Delta C_{Y,\delta_{sb}} \tag{22}$$

$$\Delta C_{Y,LG,\beta} = [C_Y(\alpha,\beta,M,LG) - C_{Y,b}(\alpha,\beta,M)] - \Delta C_{Y,LG} \tag{23}$$

Proceeding in a similar way, the rolling and yawing moment coefficients are assumed to be given by

$$\begin{aligned} C_{l,total} &= C_{l,b}(\alpha,\beta,M) + C_l(\alpha,M,\delta_a) \\ &+ C_l(\alpha,M,\delta_r) + C_l(\alpha,M,\delta_{sb}) \\ &+ C_l(\alpha,M,LG) + \Delta C_{l,\delta_r,\beta} \\ &+ \Delta C_{l,\delta_{sb},\beta} + \Delta C_{l,LG,\beta} \end{aligned} \tag{24}$$

$$\begin{aligned} C_{n,total} &= C_{n,b}(\alpha,\beta,M) + C_n(\alpha,M,\delta_a) \\ &+ C_n(\alpha,M,\delta_r) + C_n(\alpha,M,\delta_{sb}) \\ &+ C_n(\alpha,M,LG) + \Delta C_{n,\delta_r,\beta} \\ &+ \Delta C_{n,\delta_{sb},\beta} + \Delta C_{n,LG,\beta} \end{aligned} \tag{25}$$

In the above formulation, the side force ($\Delta C_{Y,LG}$), rolling and yawing moment coefficients ($\Delta C_{l,LG}$, $\Delta C_{n,LG}$) due to landing gear in zero sideslip are included because, as said earlier, the configuration is asymmetric due to the nose gear having a door only on one side. Further, note that the side force due to ailerons is included in the formulation because wind tunnel test data displayed the existence of a significant amount of side force particularly at subsonic and low supersonic speeds. A conceptual explanation for the origin of side force due to aileron (asymmetric elevons) deflection is presented in the following:

Let the right elevon be held at zero deflection and the left elevon be deflected downward (positive deflection) as shown in Figure 6. Therefore, the suction on the left wing increases compared to that on the right wing. As a result, a pressure differential comes into existence on the vertical sides of the aft fuselage (and possibly across the vertical tail) leading to a negative side force as shown in Figure 6. This side force acting aft of the moment reference point generates a positive yawing moment. Notice that this yawing moment is of opposite nature to that due to the drag differential ($\Delta C_{D,\delta_a}$) as shown in Figure 6.

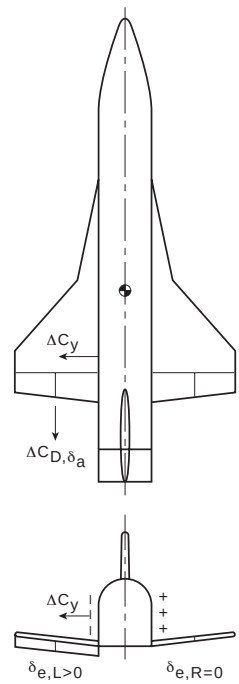

Figure 6. Conceptual explanation for side force due to aileron deflection.

Aerodynamic Coefficients in Ground Effect

Consider the vehicle operating in the proximity of the ground ($\frac{h}{b} \le 2.5$). Here, h is the height of the vehicle above the ground plane and b is the wing span. The height h is the vertical distance between the moment reference point and the ground plane. We assume that the landing gear is fully extended to its touchdown position, the main gear doors are closed and the nose gear door is open. As said before, this configuration is aerodynamically asymmetric leading to the existence of nonzero side force, rolling and yawing moments in zero sideslip.

Let C_i represent any one of the six static aerodynamic coefficients in the presence of the ground. We assume,

$$C_i(\alpha,\beta,\delta_e,\delta_{bf},\delta_{sb},\delta_a,\delta_r,\frac{h}{b}) = C_i(\alpha,\frac{h}{b}=\infty) + \Delta C_i(\alpha,\beta,\delta_e,\delta_{bf},\delta_{sb},\delta_a,\delta_r,\frac{h}{b}) \tag{26}$$

It should be noted that the inclusion of the term $\frac{h}{b}$ in the parenthesis denotes that the coefficient C_i is evaluated in ground effect. In other words, we do not treat $\frac{h}{b}$ as a new control variable. Thus, $C_i(\alpha,\frac{h}{b}=\infty)$ represents the value of the aerodynamic coefficient C_i for the baseline when the parameter $\frac{h}{b}$ becomes large, which means that the vehicle is out of ground effect or essentially in free flight.

We assume,

$$\begin{aligned}\Delta C_i(\alpha,\beta,\delta_e,\delta_{bf},\delta_{sb},\delta_a,\delta_r,\frac{h}{b}) &= \Delta C_i(\alpha,\frac{h}{b}) \\ &+ \Delta C_i(\alpha,\delta_e,\frac{h}{b}) + \Delta C_i(\alpha,\delta_{bf},\frac{h}{b}) \\ &+ \Delta C_i(\alpha,\delta_{sb},\frac{h}{b}) + \Delta C_i(\alpha,\delta_a,\frac{h}{b}) \\ &+ \Delta C_i(\alpha,\delta_r,\frac{h}{b}) + \Delta C_i(\alpha,\beta,\frac{h}{b}) \\ &+ \Delta C_i(\alpha,\beta,\delta_{sb},\frac{h}{b}) + \Delta C_i(\alpha,\beta,\delta_r,\frac{h}{b})\end{aligned} \tag{27}$$

Here, $\Delta C_i(\alpha,\frac{h}{b})$ represents the incremental coefficient C_i for baseline at an angle of attack α and zero sideslip, due to the presence of the ground (as implied by the parameter $\frac{h}{b}$ in the parenthesis) above that of the baseline in free flight and is given by,

$$\Delta C_i(\alpha,\frac{h}{b}) = C_i(\alpha,\frac{h}{b}) - C_i(\alpha,\frac{h}{b}=\infty) \tag{28}$$

The parameter $\Delta C_i(\alpha,\delta_e,\frac{h}{b})$ represents the incremental coefficient C_i due to elevon deflection at angle of attack α and zero sideslip, in the presence of the ground with respect to the baseline in the presence of the ground and at the same values of α and $\frac{h}{b}$ and is given by,

$$\Delta C_i(\alpha,\delta_e,\frac{h}{b}) = C_i(\alpha,\delta_e,\frac{h}{b}) - C_i(\alpha,\frac{h}{b}) \tag{29}$$

The present formulation of the ground effect aerodynamic model is more general than that used in the shuttle data book [14]. Further, the incremental due to ground effect is also defined in a different way. For example, the shuttle data book [14] defines the incremental due to elevon deflections in the presence of the ground as

$$\Delta' C_i(\alpha,\delta_e,\frac{h}{b}) = C_i(\alpha,\delta_e,\frac{h}{b}) - C_i(\alpha,\delta_e,\frac{h}{b}=\infty) \tag{30}$$

Here, the "prime" over the symbol "Δ" denotes the increment according to the shuttle data book [14]. The incremental due to other control surface deflections are defined in a similar way.

Thus, equation (29) gives the increment due to elevons in ground effect with respect to baseline in ground effect whereas equation (30) corresponding to the shuttle data book gives the incremental with respect to the same elevon deflection in free flight. Therefore, when $\frac{h}{b} \to \infty$, the present incremental assumes the corresponding freestream value whereas that according to the shuttle data book approaches zero.

The relation between the present values of ground effect incremental coefficients and that according to shuttle data book, say for elevon deflections, is given by

$$\begin{aligned}\Delta C_i(\alpha,\delta_e,\frac{h}{b}) &= \Delta' C_i(\alpha,\delta_e,\frac{h}{b}) - \Delta' C_i(\alpha,\frac{h}{b}) \\ &+ [C_i(\alpha,\delta_e,\frac{h}{b}=\infty) \\ &- C_i(\alpha,\frac{h}{b}=\infty)]\end{aligned} \tag{31}$$

Note that

$$\Delta' C_i(\alpha,\frac{h}{b}) = \Delta C_i(\alpha,\frac{h}{b}) \tag{32}$$

Thus, we observe that the present method of defining the ground effect incremental coefficients is a little more convenient for building the ground effect aerodynamic model by adding the increments due to various control deflections.

The incremental coefficients due to bodyflap, speedbrake, ailerons and rudder at angle of attack α and zero sideslip are defined as,

$$\Delta C_i(\alpha,\delta_{bf},\frac{h}{b}) = C_i(\alpha,\delta_{bf},\frac{h}{b}) - C_i(\alpha,\frac{h}{b}) \tag{33}$$

$$\Delta C_i(\alpha,\delta_{sb},\frac{h}{b}) = C_i(\alpha,\delta_{sb},\frac{h}{b}) - C_i(\alpha,\frac{h}{b}) \tag{34}$$

$$\Delta C_i(\alpha,\delta_a,\frac{h}{b}) = C_i(\alpha,\delta_a,\frac{h}{b}) - C_i(\alpha,\frac{h}{b}) \tag{35}$$

$$\Delta C_i(\alpha,\delta_r,\frac{h}{b}) = C_i(\alpha,\delta_r,\frac{h}{b}) - C_i(\alpha,\frac{h}{b}) \tag{36}$$

Now consider the incremental coefficients involving sideslip β. The incremental coefficients due to sideslip are defined as,

$$\Delta C_i(\alpha,\beta,\frac{h}{b}) = C_i(\alpha,\beta,\frac{h}{b}) - C_i(\alpha,\frac{h}{b}) \tag{37}$$

$$\begin{aligned}\Delta C_i(\alpha,\beta,\delta_r,\frac{h}{b}) &= [C_i(\alpha,\beta,\delta_r,\frac{h}{b}) \\ &- C_i(\alpha,\beta,\frac{h}{b})] \\ &- \Delta C_i(\alpha,\delta_r,\frac{h}{b})\end{aligned} \tag{38}$$

$$\begin{aligned}\Delta C_i(\alpha,\beta,\delta_{sb},\frac{h}{b}) &= [C_i(\alpha,\beta,\delta_{sb},\frac{h}{b}) \\ &- C_i(\alpha,\beta,\frac{h}{b})] \\ &- \Delta C_i(\alpha,\delta_{sb},\frac{h}{b})\end{aligned} \tag{39}$$

Note that

$$\begin{aligned}C_i(\alpha,\beta,\frac{h}{b}) &= C_i(\alpha,\frac{h}{b}=\infty) \\ &+ \Delta C_i(\alpha,\frac{h}{b}) + \Delta C_i(\alpha,\beta,\frac{h}{b})\end{aligned} \tag{40}$$

Then, the equation (26) can be expressed as,

$$\begin{aligned}C_i(\alpha,\beta,\delta_e,\delta_{bf},\delta_{sb},\delta_a,\delta_r,\frac{h}{b}) &= C_i(\alpha,\beta,\frac{h}{b}) \\ &+ \Delta C_i(\alpha,\delta_e,\frac{h}{b}) + \Delta C_i(\alpha,\delta_{bf},\frac{h}{b}) \\ &+ \Delta C_i(\alpha,\delta_{sb},\frac{h}{b}) + \Delta C_i(\alpha,\beta,\delta_{sb},\frac{h}{b}) \\ &+ \Delta C_i(\alpha,\delta_a,\frac{h}{b}) + \Delta C_i(\alpha,\delta_r,\frac{h}{b}) \\ &+ \Delta C_i(\alpha,\delta_r,\beta,\frac{h}{b})\end{aligned} \tag{41}$$

Note that the suffix of the coefficient C_i takes values from 1 to 6, for six components of aerodynamic forces and moments (C_L, C_D, C_m, C_Y, C_l, C_m).

Process of Development of the Aerodynamic Database

The above formulations of the aerodynamic model for the free flight and ground effect provide a frame work for building the aerodynamic database. The X-34 database consists of aerodynamic data tables in the form of total and incremental coefficients. The data is provided in a convenient form so that the user can evaluate each of the terms appearing in the free flight and ground effect aerodynamic models and then sum all the terms to get the desired aerodynamic coefficient.

The aerodynamic data in the aero database is presented for several Mach numbers from 0.3 to 9.0 with closely spaced values in the transonic regime. The ground effect aerodynamic data is presented for M = 0.3 with $\frac{h}{b}$ varying from 0.2 to 2.5. The angle of attack varies from –6° to 21° for M = 0.3 to 2.5 and from –5° to 40° for M = 3.0 to 9.0. The data is presented for elevon deflections of –30° to 20°, aileron deflections from –30° to +20° (left elevons deflected, right held at zero), bodyflap deflections of –15° to 20°, rudder deflections from –5° to –20° and nominal speedbrake deflections from 30° to 90°. The sideslip ranges from –4° to +5°.

As stated earlier, the current X-34 program started in the Summer of 1996. At that time, some preliminary wind tunnel test data at low subsonic (M = 0.2) and hypersonic Mach numbers (M = 6) were available for the previous (cancelled) X-34 configuration. While the wind tunnel tests on the new X-34 configuration were yet to start, it was necessary to quickly put together an aero database for the GN&C community to get started with the flight control system design. For this purpose, the first version of the aero database was developed using APAS and adjustments to APAS results were made using the available wind tunnel data (at M = 0.2 and 6.0). For other Mach numbers, past experience with similar vehicles such as the Space Shuttle and wing-body configurations was used to adjust the APAS predictions [11,12,13].

The database was updated as the wind tunnel test results on the current X-34 model became available from the 16-Foot Transonic Tunnel, Unitary Plan Wind Tunnel, and the 14- by 22-Foot Subsonic Tunnel tests. The APAS results were replaced with the actual wind tunnel test data wherever available. At some Mach numbers like 1.1 and 1.4 where data was required but the wind tunnel test data was not available, smooth interpolations using Matlab [15] were done to obtain the aerodynamic coefficients. For M ≥ 6.0, where wind tunnel test data is not yet available, APAS was used to adjust the Mach 6 wind tunnel test data for Mach 7 to 9. This was done by adding the incrementals due to Mach number variations (all other parameters kept constant) derived from APAS to the Mach 6 test data. For example,

$$C_i(\alpha, Mach\,7) = C_i(\alpha, Mach\,6, WT) + \Delta C_i(APAS) \tag{42}$$

where

$$\Delta C_i(APAS) = C_i(\alpha, Mach\,7, APAS) - C_i(\alpha, Mach\,6, APAS) \tag{43}$$

and so on. Currently, the Mach 10 tests on the X-34 model are underway at NASA Langley. The database will be further updated when these results become available.

Results and Discussion

The variation of lift and drag coefficients of the baseline vehicle are presented in Figure 7. The angle of attack extends up to 20° for Mach 0.3 to 2.5 and to 35 ° for M = 3.0 to 9.0. We observe that the lift coefficient steadily increases from α = 0 to 20° for Mach 0.3 to 2.5 indicating that the vehicle does not stall up to 20° in this Mach range. Similarly, at higher Mach numbers, the stall is not encountered up to α = 35°. We observe that, for a given value of alpha, the drag coefficient displays the usual transonic drag rise with a peak value around Mach 1.05 and then a gradual decrease for further increases in Mach number.

The variation of the pitching moment coefficient at various Mach numbers is presented in Figure 8. We observe that at low subsonic speeds (Mach 0.3), the vehicle is unstable in pitch at low α,

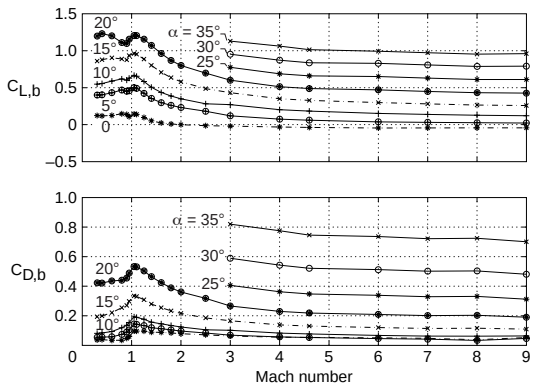

Figure 7. Variation of lift and drag coefficients for the baseline configuration with Mach number for various angles of attack.

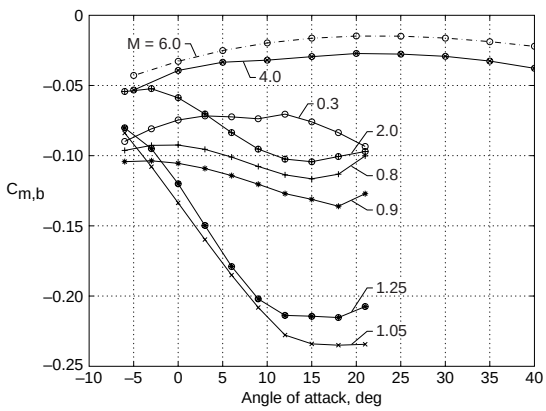

Figure 8. Variation of pitching moment coefficient for the baseline configuration with angle of attack for various Mach numbers.

exhibits a sharp pitch up tendency around $\alpha = 9°$ and then a stable break with further increase in α. As the Mach number increases above 0.3, the angle of attack at which pitch up occurs also increases as observed in Figure 8. At transonic and supersonic speeds, the vehicle becomes stable due to the aft movement of the center of pressure. As Mach number increases further, the vehicle becomes unstable once again on account of the increasing lift developed by the forward parts of the fuselage. However, the pitching moment coefficient displays a tendency for a stable break at high angles of attack when the stabilizing moment due to the wings exceeds the unstable moment due to the forward parts of the fuselage. This type of variation in pitching moment coefficient is typical of wing-body configurations at hypersonic speeds.

An example of elevon effectiveness from subsonic to hypersonic speeds is shown in Figure 9 for $\alpha = 6°$. An anomaly observed here is that around Mach 0.95, an elevon deflection from –10° to –20° deflection gives a smaller increment in pitching moment coefficient compared to that from –20° to –30°. This was accompanied by the same effect on the lift coefficient. Some additional tests conducted at the polysonic wind tunnel of NASA Marshall Space Flight Center also confirmed this phenomenon observed in Langley 16-Foot transonic wind tunnel tests. While it can be speculated that this phenomenon may be due to some type of shock wave and boundary layer interaction, precise reasons for this discrepancy are not clear at this stage because flow diagnostic tests were not conducted due to the fast-paced nature of the wind tunnel test program. This anomaly existed for low angles of attack and disappeared for higher angles of attack.

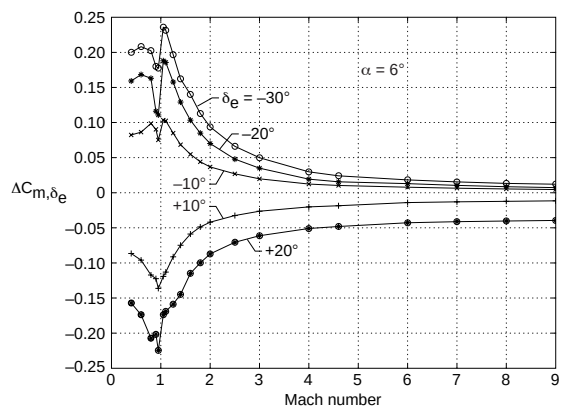

Figure 9. Variation of incremental pitching moment coefficient due to elevons with Mach number at $\alpha = 6°$.

The variation of bodyflap effectiveness for $\alpha = 6°$ is shown in Figure 10. The data for the bodyflap deflection of –15° goes only up to Mach 4.6. It is observed that the positive (downward) deflections of the bodyflap produce relatively higher increments in pitching moment compared to negative (upward) deflections.

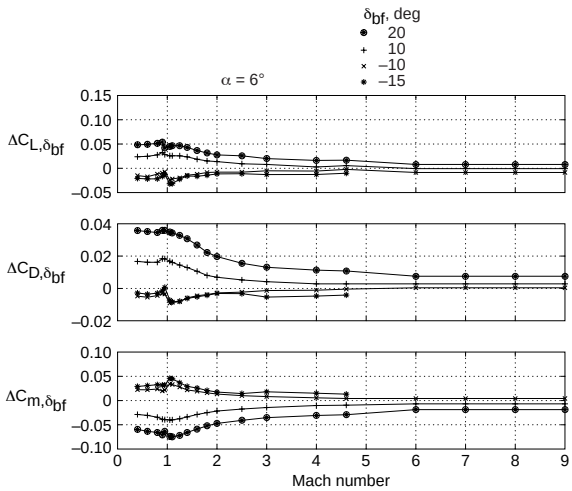

Figure 10. Variation of incremental pitching moment coefficient due to body flap with Mach number at $\alpha = 6°$.

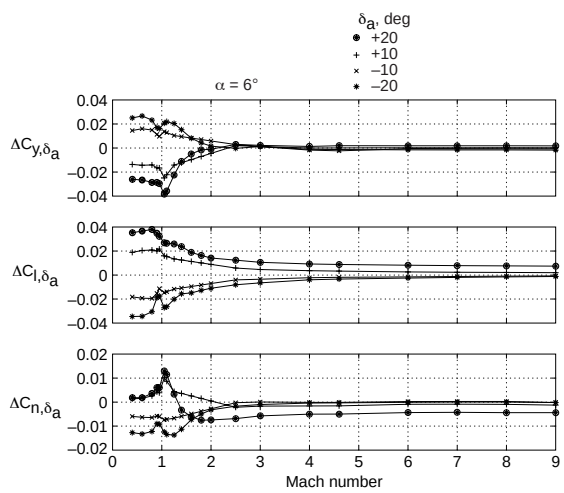

Figure 11. Variation of incremental side force, rolling and yawing moment coefficients due to aileron with Mach number at $\alpha = 6°$.

Typical aileron effectiveness is shown inFigure11 for $\alpha = 6°$. The aileron effectiveness as measured by the rolling moment coefficient steadily decreases as Mach number increases. It is observed that significant side force exists especially at subsonic and low supersonic speeds due to aileron deflections and this effect has been included in the aerodynamic model as discussed earlier. Notice that the side force tends to vanish for $M \geq 2$. The vanishing of the side force is associated with a sign change in the yawing moment for aileron deflections of 10° and 20° which is consistent with the conceptual explanation given earlier.

The rudder effectiveness as measured by the yawing moment coefficient decreases rapidly at high Mach numbers as shown in Figure 12. The speedbrake effectiveness as measured by the drag incremental also diminishes at higher Mach numbers as shown in Figure 13. The increment in drag due to speedbrake is also accompanied by an increase in pitching moment (noseup) and can be used to augment pitch control. It was found that for a given Mach number, both rudder and speedbrake lost their effectiveness at high angles of attack. Thus, a combination of high angle of attack and high Mach number leads to a rapid loss of rudder and speed-

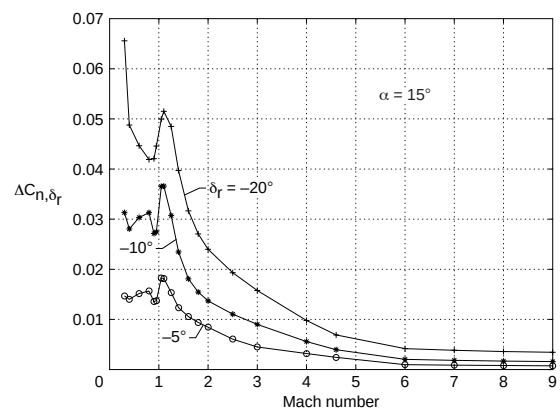

Figure 12. Variation of incremental yawing moment coefficient due to rudder with Mach number.

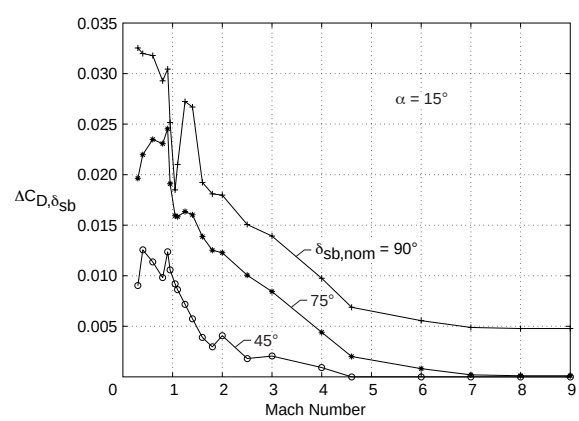

Figure 13. Variation of incremental drag coefficient due to speedbrake with Mach number.

brake effectiveness. This loss of effectiveness is usually due to the immersion of these control surfaces in the low energy wake of the fuselage and wings. When this happens, the X-34 flight vehicle may require the use of reaction control system for directional control.

The rolling and yawing moment coefficients due to baseline in sideslip for $\alpha = 6°$ are shown in Figure 14. It is observed that at this angle of attack, the vehicle is stable in roll ($C_{l\beta} < 0$) for Mach numbers up to about 1.7 and beyond this Mach number, the vehicle becomes unstable in roll ($C_{l\beta} > 0$).This behavior was found to exist for angles of attack from 0 to 15°. Beyond 15° angle of attack, the vehicle becomes stable in roll at all Mach numbers (except for Mach numbers close to 1.0) due to the increasing stabilizing effect of the wing dihedral. At $\alpha = 9°$, the vehicle is directionally stable ($C_{n\beta} > 0$) up to Mach 1.5 and unstable for higher Mach numbers as shown in Figure 14. It was noted that for $\alpha > 12°$, the vehicle becomes directionally unstable at all Mach numbers.

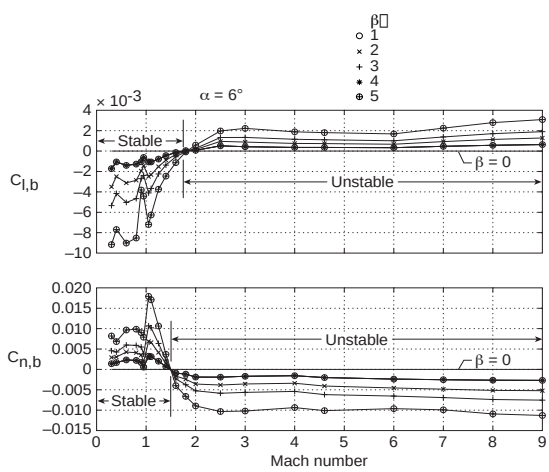

Figure 14. Variation of rolling and yawing moment coefficients with Mach number for the baseline configuration in sideslip at $\alpha = 6°$.

The yawing moment coefficient displayed an interesting variation for small values of sideslip at transonic Mach numbers. An example of this variation is shown in Figure 15. The vehicle is unstable around $\beta = 0$ but becomes stable as sideslip increases. The physical causes of this behavior in yawing moment are not clear at this stage because as stated earlier, flow diagnostic tests were not conducted in this study. This may not be a major concern because the destabilizing effect is localized around $\beta = 0.5$ and for higher sideslip, the vehicle becomes stable.

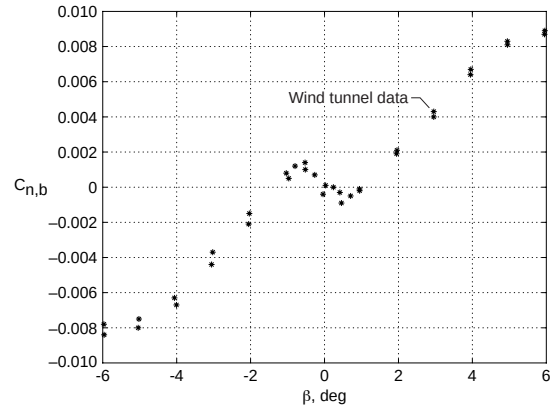

Figure 15. Variation of yawing moment coefficient of the baseline configuration with sideslip for $M = 0.95$ and $\alpha = 0$.

The effect of landing gear deployment at low subsonic speeds on pitching moment is shown in Figure 16. It is observed that the landing gear deployment leads to a more nose down pitching moment at low angles of attack. For angles of attack above 12°, the trend reverses. The proposed angle of attack during approach to landing is around 12° and it is observed that the associated incremental nose down pitching moment is quite small.

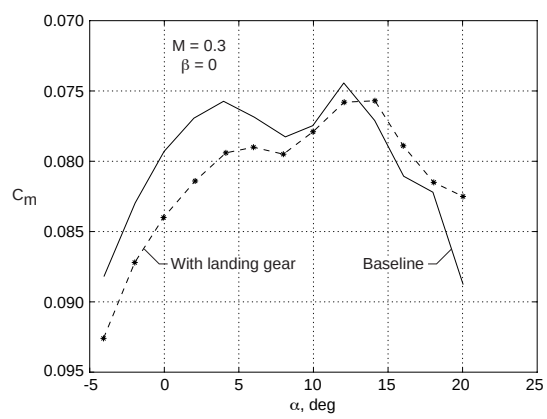

Figure 16. Effect of landing gear deployment on pitching moment coefficient.

The effects of combined sideslip and landing gear deployment are shown in Figure 17. It is observed that the vehicle experiences a significant loss of directional stability due to landing gear deployment. Also, it can be noted that a significant asymmetry in pitching moment coefficient exists with sideslip apparently due to the aerodynamic asymmetry caused by the single nose gear door.

The ground effect aerodynamic data for the baseline configuration are shown in Figure 18. It is observed that the incremental lift and drag coefficients are positive whereas the pitching moment increments are negative. This is to be expected since in the presence of the ground, the strength of the tip vortices diminishes leading to a general reduction in downwash and higher effective angles of attack along the wing span.

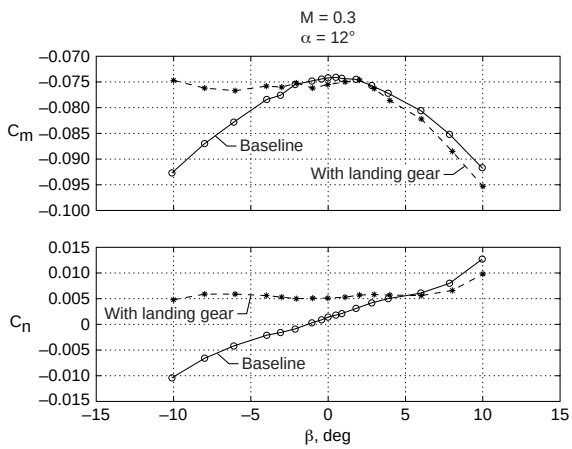

Figure 17. Combined effect of landing gear and sideslip at M = 0.3, α = 12°.

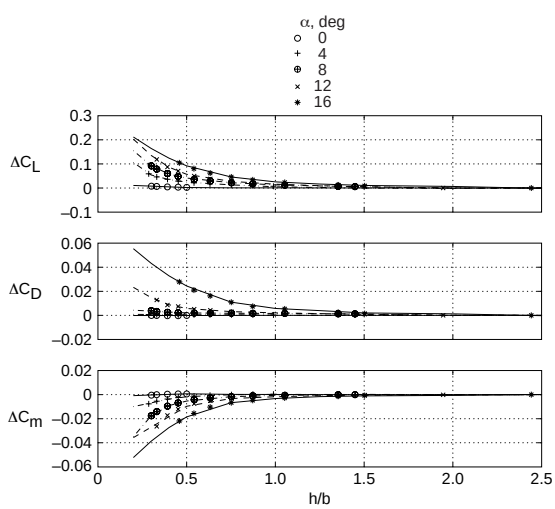

Figure 18. Incremental lift, drag and pitching moment coefficients due to baseline configuration in ground effect.

The incremental pitching moment coefficient for a typical elevon deflection of –10° in ground effect are shown in Figure 19. It can be observed that in the presence of the ground, the elevons become more effective due to the general reduction in downwash as said before. The ground effect was found to be similar on bodyflap deflections. It was noted that the presence of the ground does not have much effect on the rolling and yawing moments due to aileron deflections. The ground effect on the vehicle in sideslip was small except at high values of sideslip near 8° which may be encountered during landings with cross winds in excess of 50 ft/sec.

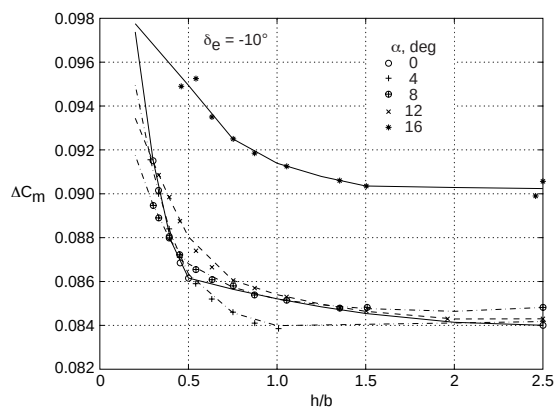

Figure 19. Incremental pitching moment coefficient due to –10° elevons in ground effect.

The ground effect test data was obtained for some combinations of angles of attack, elevon, bodyflap and speedbrake deflections. These data can be used as validation tests for the ground effect aerodynamic model. The results of this exercise are shown in Figure 20. It is observed that the agreement of the computed aerodynamic coefficients is within 5 or 6% of the wind tunnel test data. The good agreement indicates that the mutual interference between various control surfaces is small as assumed in development of the ground effect aerodynamic model. However, such an exercise was not

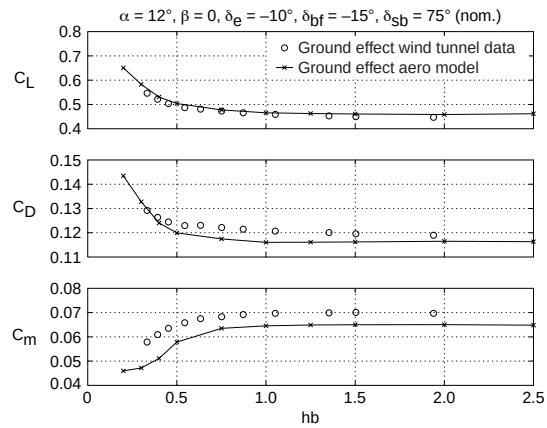

Figure 20. Validation test for ground effect aerodynamic model.

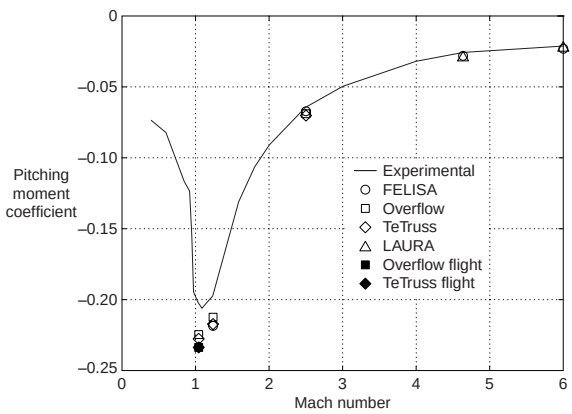

Figure 21. Pitching moment coefficient at tunnel and flight Reynolds numbers.

done for free flight aerodynamic model due to the non availability of similar type of test data.

The test Reynolds numbers for the X-34 model (based on mean aerodynamic chord) range up to 2×10^6 whereas corresponding full scale flight Reynolds numbers range up to 40×10^6. The test Reynolds numbers match the flight Reynolds numbers only for a segment of the hypersonic descent. Elsewhere, the flight Reynolds numbers are orders of magnitude higher than the test Reynolds numbers. To assess the impact of this, Langley has done a limited exercise using various CFD codes. The modern CFD codes are capable of making very good predictions of lift and drag coefficients. It is the prediction of pitching moment coefficients that presents a challenge to the CFD codes. The accurate prediction of pitching moment coefficient for full scale flight Reynolds numbers is of critical importance from pitch trim considerations. The results of this exercise are shown in Figure 21. It is observed that all the CFD codes predict the pitching moment coefficient reasonably well at the tunnel Reynolds numbers as shown by open symbols. With this kind of code "calibration", two CFD codes were used to predict pitching moment coefficient at flight Reynolds numbers as shown by filled symbols. Comparing corresponding values of pitching moment coefficient for tunnel and flight Reynolds numbers, it is observed that the flight test vehicle is likely to experience a slightly higher nosedown pitching moment than predicted by the wind tunnel tests and hence the data in the aero database.

The control history for the DRM2 trajectory of Figure 3 based on a simulation using the present aerodynamic database is shown in Figure 22. The thrust vectoring (gimbal angle) of about 15° is used initially during the ascent. The speedbrake is open at about 75° during the initial part of the ascent mainly to provide noseup pitch control and during the descent for energy management. The bodyflap is held constant at –10°. The elevon deflections are always negative (upward) and reach a minimum value of –22°. At this point in the trajectory, the vehicle has a small margin in pitch control to deal with disturbance rejection and other uncertainties such as Reynolds number effects.

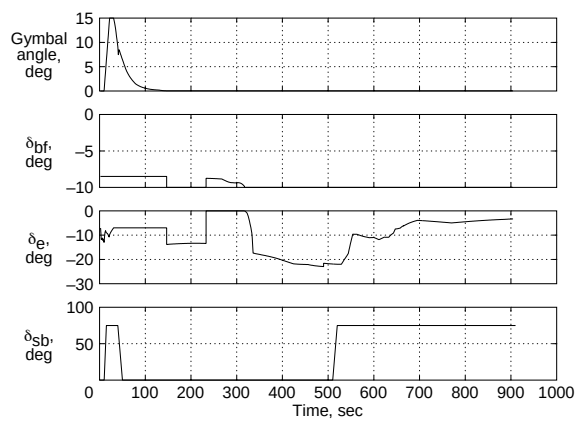

Figure 22. Control history for the nominal trajectory.

Concluding Remarks

We have presented an overview of the wind tunnel tests, aerodynamic analyses and the process of development of the preflight aerodynamic database of the NASA/Orbital X-34 reusable launch vehicle from subsonic to hypersonic Mach numbers. This aerodynamic data is provided for both free flight and flight in ground effect and covers the complete range of Mach numbers, angles of attack, sideslip and control surface deflections anticipated in the entire flight envelope of the X-34 vehicle. This aerodynamic data is in a form suitable for flight control system design. A typical control history based on the application of the present aerodynamic database shows that the vehicle has satisfactory control capabilities at all the points along the nominal flight trajectory.

Acknowledgement

Authors are thankful to Henri Fuhrman, Dan Rovner and Mike Ruth of Orbital for the nominal trajectory and control history, and to Jim Weilmuenster. Ken Sutton, Peter Buening, Ram Prabhu and Shahyar Pirzadeh of NASA Langley for the CFD calculations.

References

1) Freeman, D.C. Jr., Talay, T.A., and Austin R.E.: *Reusable Launch Vehicle Technology Program*, IAF 96-V.4.01, October 1996.

2) NASA: *Reusable Launch Vehicle (RLV), Small Reusable Booster, X-34*, Cooperative Agreement Notice, CAN 8-2, January 1995.

3) Wurster, K. E., Riley C.J., and Vincent Zoby E.; *Engineering Aerothermal Analysis for X-34 Thermal Protection System Design*, AIAA Paper 98-0882, January 1998.

4) Gentry, C. E., Quinto, P.F., Gatlin, G.M., Gregory, M., and Applin, Z.T.: *The Langley 14- by 22- Foot Subsonic Tunnel: Description, Flow Characteristics and Guide for Users*, NASA TP-3008, September 1990.

5) Capone, F.J., Bangert, L.S., Asbury, S.C., Mills, C.T., and Bare, E.A.: *The NASA Langley 16- Foot Transonic Tunnel*, NASA TP-3521, September 1995.

6) Jackson, C.M., Corlett, W.A., and Monta, W.J.: *Description and Calibration of the Langley Unitary Plan Wind Tunnel*, NASA TP-1905, November 1981.

7) Micol, J.M.: Hypersonic Aerodynamic/Aerothermodynamic Testing Capabilities at Langley Research Center: Aerodynamic Facilities Complex, AIAA Paper 95-2107, 1995.

8) Brauckmann, G.J.: *X-34 Vehicle Aerodynamic Characteristics*, AIAA Paper 98-2531, January 1998.

9) Bonner, E., Clever, W., and Dunn, K.: *Aerodynamic Preliminary Analysis System II, Part I – Theory*, NASA CR-165627, 1989.

10) Divan, P., and Sova, G.: *Aerodynamic Preliminary Analysis System II, Part II- User's Manual*, NASA CR-165628, 1989.

11) Cruz, C., and Wilhite, A.: *Prediction of High-Speed Aerodynamic Characteristics Using Aerodynamic Preliminary Analysis System (APAS),* AIAA Paper No. 89-2173, 1989.

12) Cruz, C., and Ware, G.: *Predicted Aerodynamic Characteristics for HL-20 Lifting Body Using the Aerodynamic Preliminary Analysis System (APAS)*, AIAA Paper No. 92-3941, 1992.

13) Cruz, C., and Engelund, W.C.: *An Aerodynamic Preliminary Analysis System (APAS) Calibration Report: Space Shuttle Orbiter*, Paper presented at the Society of Hispanic Professional Engineers 6th Annual Eastern Technical and Career Conference, Washington D.C., November 12-14, 1992.

14) Rockwell International Space Division.: *Aerodynamic Design Data Book, Vol. I, Orbiter Vehicle*, Report No. SD 72-SH-0060-1L, November 1977.

15) *Pro-Matlab for Sun Work Stations*, The Math Works, Natick, MA, January 1990.